Disrupted white matter microstructure in chronic Zika virus-infected adults

Suhnyoung Jun[1,2], Richard Bido-Medina[3], Jairo Oviedo[4], Isidro Miches[5], Daniel Llano[1], Luis Tusen[6], Peter Stoeter[4,7], Minelly Rodriguez[6], Sepideh Sadaghiani[1,2,8]

1 Beckman Institute for Advanced Science and Technology, University of Illinois at Urbana-Champaign, Urbana, Illinois
2 Department of Psychology, University of Illinois at Urbana-Champaign, Urbana, Illinois, United States
3 Department of Psychiatry, Massachusetts General Hospital, Harvard Medical School, Boston, Massachusetts
4 Centro Gamma Knife Dominicano, Centro Diagnostico de Medicina Avanzada y Telemedicina (CEDIMAT), Santo Domingo, Dominican Republic

5 Department of Surgery, Hospital Docente Salvador B. Gautier. Santo Domingo Dominican Republic.

6 Department of Neurology, Hospital Salvador B. Gautier, Santo Domingo, Dominican Republic

7 Department of Radiology, CEDIMAT, Santo Domingo, Dominican Republic

8 Neuroscience Program, University of Illinois at Urbana-Champaign, Urbana, Illinois, United States

Keywords: Zika virus, Guillain-Barre Syndrome, Central Nervous System (CNS), Viral Encephalitis, Diffusion tensor imaging

Data Availability: The dataset supporting the findings of this study is publicly available on the **Illinois Data Bank**. The data include demographic and clinical information of the subjects, structural and functional neuroimaging data and relevant metadata collected as part of this study on the impact of the Zika virus on the human adult brain. Researchers can access the dataset at the following DOI: https://doi.org/10.13012/B2IDB-5584114_V1. The data are provided under the CC BY 4.0 license, allowing for reuse with proper attribution. Any additional details on data usage and accessibility can be found in the repository documentation.

Abstract (NeuroImage:Clinical- 250 words)

Systemic viral infections with neurotropic potential continue to pose significant global health challenges. The Zika virus (ZIKV) is known for its pronounced neurotropism. Research on ZIKV has predominantly centered on congenital and infant populations, where the virus' detrimental effects on brain development are well-documented. However, increasing evidence suggests that the mature central nervous system (CNS) is also susceptible to ZIKV. Despite this, no study has comprehensively investigated the potential long-term structural and functional changes in the adult human brain.

To address this gap, we studied a group of rare adult ZIKV patients presenting with both peripheral and, importantly, CNS-related neurological symptoms. We compared these patients to healthy controls and to patients with Guillain-Barre Syndrome of non-ZIKV etiology, which predominantly affects the peripheral nervous system. Here, we focused on structural (cortical thickness, white matter hyperintensities, and diffusion measures) and functional (hippocampus-dependent resting state connectivity) changes in the brain associated with ZIKV at the chronic stage, i.e. 5 to 12 months from the infection.

We observed decreased mean diffusivity in the inferior fronto-occipital fasciculus and the forceps major in the ZIKV-CNS-GBS group compared to other groups. Notably, some of the CNS-related neurological symptoms of the ZIKV patients corresponded with the functional role of these affected white matter tracts. However, we found no evidence for long-term changes in cortical thickness, white matter hyperintensities, or functional connectivity.

Our findings suggest that the more pronounced and prolonged changes in white matter, compared to gray matter, may reflect the greater metabolic demands and prolonged timecourse of white matter repair, particularly in the context of inflammation and oxidative stress in the brain associated with ZIKV infection. This case-control study provides first evidence for the long-term impact of ZIKV infection on the adult human brain, emphasizing the importance of extending ZIKV research and health policy considerations to the adult population.

1. Introduction

The Zika virus (ZIKV), a neurotropic flavivirus, gained global attention following its explosive spread across French Polynesia and the Americas in 2015 (Rasmussen et al., 2016). As of December 2022 (most recent WHO report; World Health Organization (WHO), 2022), a total of 89 countries and territories have documented evidence of autochthonous mosquito-borne transmission of ZIKV. While initial outbreaks were primarily associated with severe birth defects such as fetal microcephaly, it has become clear that ZIKV's impact extends far beyond congenital infections. Particularly in adults, ZIKV has been implicated in a wide range of neurological disorders, including Guillain-Barré syndrome (GBS), an immune-mediated neuropathy of the *peripheral* nervous system (Cao-Lormeau et al., 2016; Dos Santos et al., 2016; Munoz et al., 2016, 2017; Parra et al., 2016; da Silva et al., 2017).

Specifically, a previous study has demonstrated the presence of the ZIKV RNA genome in patients with presumed ZIKV-GBS, with a significant proportion showing ZIKV detected by reverse transcription polymerase chain reaction (RT-PCR) and other serological analyses in different bodily fluids (e.g., blood, cerebrospinal fluids (CSF), and urine) (Parra et al., 2016). The study further showed that 43% of ZIKV-GBS had neurological symptoms occurring concurrently or shortly after the onset of ZIKV symptoms. This suggests that ZIKV-associated GBS may follow the pattern of a para-infectious disorder rather than the classic postinfectious profile of GBS from other etiology (Parra et al., 2016; Munoz et al., 2017).

The spectrum of ZIKV-associated neurological diseases in adults is not limited to GBS but may extend to the *central* nervous system (CNS), such as encephalopathy, encephalitides, meningitis, myelitis, and seizures (Carteaux et al., 2016; Galliez et al., 2016; da Silva et al., 2017). Despite the evident link between ZIKV and CNS-related neurological symptoms, neuroimaging evidence for the impact of ZIKV on the adult brain has been largely limited to case reports, focusing on the diagnosis and the prognosis of neurological symptoms (Carteaux et al., 2016; Galliez et al., 2016; da Silva et al., 2017; Pradhan et al., 2017; Sebastian et al., 2017). Moving beyond case studies, the first case-control neuroimaging group study provided evidence for the impact of subacute ZIKV infection on changes in gray matter volume and resting-state functional connectivity (RSFC) networks (Bido-Medina et al., 2018). However, the long-term impact of chronic ZIKV infection on the adult brain structure and function is still missing.

Animal studies with adult murine models have demonstrated that ZIKV infection, administered through intraperitoneal (Aliota et al., 2016; Kim et al., 2020), subcutaneous (Dowall et al., 2016), or intravenous (Papa et al., 2017; Leda et al., 2019) routes, may lead to brain infection. Specifically, *in vitro* studies have shown that ZIKV preferentially infects neural progenitor cells over mature neurons (Sutarjono, 2019), making hippocampal structures susceptible to reduced cell proliferation, elevated pro-inflammatory cytokines and astrocytic reaction, premature apoptosis, and autophagy (Li et al., 2016; Souza et al., 2016; Devhare et al., 2017; Zhou et al., 2017; Büttner et al., 2019; Figueiredo et al., 2019; Garber et al., 2019; Bobermin et al., 2020). Some speculated that this neurotropic effect stems from the similarities between the ZIKV genome sequence and the retinoic acid response element (RARE), a well-known early neural tube developmental marker (Kumar et al., 2016).

Further, investigations on the potential mechanisms of ZIKV crossing into the brain suggest that the virus may exploit multiple pathways, including the blood-CSF barrier and the blood-brain barrier (BBB). Notably, non-intracranial injection of ZIKV in adult mice has been shown to infect pericytes in the choroid plexus, compromising the blood-CSF barrier and facilitating viral dissemination into the cortex following CSF entry (Kim et al., 2020). Additionally, ZIKV may cross the BBB through basolateral release, transcytosis, or transinfection from infected endothelial cells, without necessarily disrupting BBB integrity (Papa et al., 2017).

In addition to these direct viral pathways of CNS infection, ZIKV may indirectly impact the CNS through complex immune-mediated mechanisms. Studies have revealed that ZIKV infection can trigger the production of autoantibodies targeting peripheral nerve antigens, which may potentially cross-react with CNS structures (Rivera-Correa et al., 2019; Davies et al., 2022). Notably, ZIKV-associated GBS patients showed higher levels of anti-glycolipid antibodies compared to ZIKV-infected patients without GBS, targeting a broad repertoire of gangliosides with both IgM and IgG responses (Cao-Lormeau et al., 2016; Rivera-Correa et al., 2019; Davies et al., 2022). The heterogeneous nature of these autoantibody responses suggests a broad spectrum of immune reactions that could indirectly affect the CNS. Furthermore, ZIKV infection has been associated with complement activation, as evidenced by similarities between ZIKV E protein and human complement component C1q, along with the presence of anti-C1q antibodies in ZIKV-infected animals (Koma et al., 2018; Jeong et al., 2023). This complement-mediated inflammation, coupled with elevated brain levels of pro-inflammatory cytokines and microglial activation, may further contribute to CNS pathology (Figueiredo et al., 2019).

While these findings underscore ZIKV's neurotropic potential and its capacity to induce persistent neuronal damage through both direct and indirect mechanisms, the long-term impact of the ZIKV infection on the human adult brain's structure and function remains largely unexplored. Therefore, our study addresses this critical knowledge gap by presenting the first case-control neuroimaging investigation into the chronic impact of ZIKV on brain structure and function in adults. Specifically, we explore white and grey matter integrity as well as intrinsic functional connectivity in patients with chronic ZIKV-associated CNS symptoms (ZIKV-CNS-GBS). In terms of structure, we studied changes in cortical thickness, white matter lesions, and white matter integrity via diffusion weighted metrics. In terms of integrity of the brain's functional connectivity architecture, we focused on the hippocampus as a seed due to its known susceptibility to the ZIKV (see above).

Notably, the current study employed two different control groups: age- and sex-adjusted healthy controls to establish a neurologically healthy baseline and study brain alterations independent of normal demographic variation; and patients with GBS but without ZIKV etiology (NZIKV-GBS) to identify brain alterations specific to ZIKV-CNS manifestations that are independent of GBS. By focusing on chronic-stage patients, the present study aims to elucidate the long-term structural and functional brain disruptions associated with ZIKV, advancing our understanding of the ZIKV's lingering neurological effects and potential clinical characterization.

2. Materials and Methods

Figure 1 is a schematic representation of the overall approach and analysis subsections. Our study included a comprehensive set of structural features and employed a consistent analytical approach to investigate the long-term effect of adult ZIKV infection on structural and functional changes.

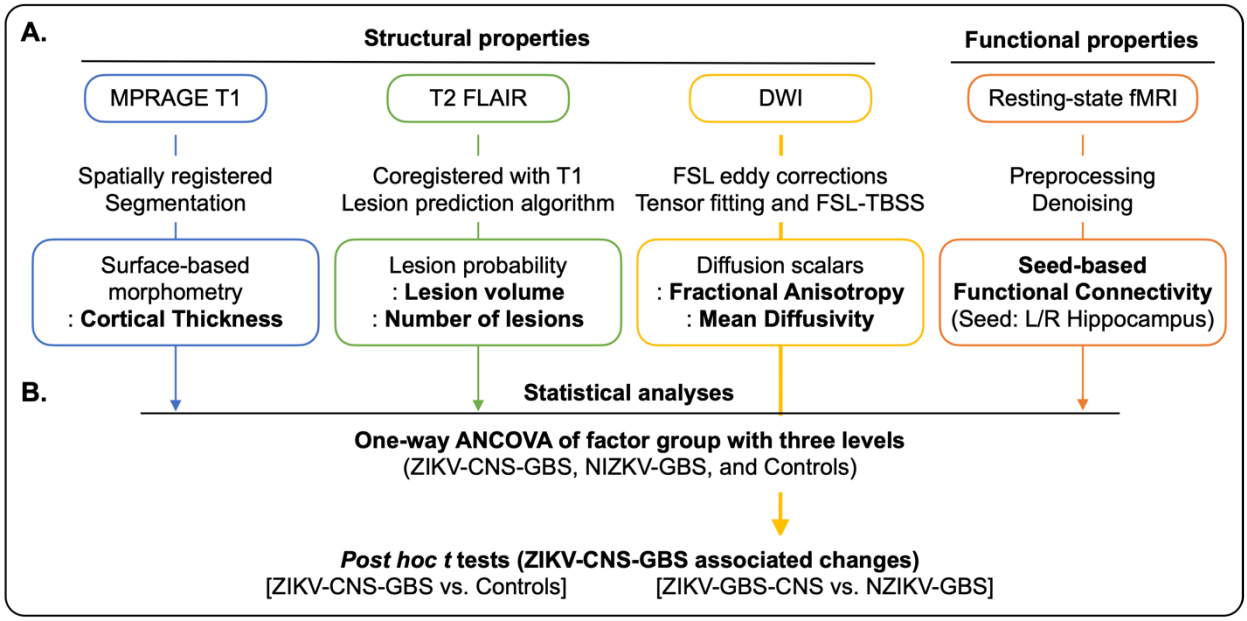

Figure 1. An overview of the analysis pipeline. This figure illustrates the workflow for analyzing multiple neuroimaging modalities. (A) For each modality, we performed preprocessing and extracted key structural and functional features. Specifically, we assessed cortical thickness using surface-based morphometry, lesion characteristics through lesion probability mapping, diffusion metrics (including fractional anisotropy and mean diffusivity), and seed-based functional connectivity. (B) Each of these features was then subjected to a one-way ANCOVA to examine group differences across three cohorts: adults with confirmed ZIKV-associated CNS and GBS symptoms (ZIKV-CNS-GBS), adults with non-ZIKV-related GBS (NZIKV-GBS), and healthy controls. Subsequent to significant *F*-test results, *post hoc t*-tests were applied to further explore the specific effects across groups.

2.1. Participants

We recruited 14 adult patients (6 females; age = 34.93 (± 8.14) years) with confirmed ZIKV infection and ZIKV-associated CNS-related neurological symptoms and GBS manifestations (ZIKV-CNS-GBS), 15 adult patients (5 females; age = 43.21 (±9.37) years) with GBS manifestations without ZIKV etiology (NZIKV-GBS), and 14 healthy controls (6 females; age = 32.21 (±4.98) years). All subjects were recruited in the Dominican Republic, endemic to Aedes mosquito-borne diseases. Recruitment and clinical assessment occurred at Hospital Salvador B. Gautier, in Santo Domingo, and MRI data were acquired at Centro de Diagnóstico Medicina Avanzada y Telemedicina (CEDIMAT), Santo Domingo, Dominican Republic. All subjects gave written informed consent according to procedures approved by the Internal Review Boards of the University of Illinois at Urbana-Champaign, IL, USA, Hospital Gautier, and CEDIMAT. All patients presented an abrupt onset of neurological deterioration with variable periods between systemic manifestation and neurological symptoms. Only patients with stable cognitive and clinical status (Mini-Mental State Examination >= 23 and Glasgow scale >= 13) underwent the MRI scan.

All patients were diagnosed with a GBS-like syndrome by clinical manifestations and electromyography (EMG), and CSF testing was performed (i.e., albumin-cytologic dissociation) in 18 of the patients (i.e., 10 ZIKV-CNS-GBS patients and 8 NZIKV-GBS patients). Nerve velocity conduction using EMG (EMG/ NVC) was assessed by investigator L.T. during the acute stage. HIV status was assessed using ELISA and was reported negative for all patients. Disability due to the radiculopathy was

measured by Hughes modified scale at admission and discharge. In accordance with the Dominican Protocol (2016) for the management of GBS, patients were treated with immunoglobulins (2 g/kg divided in 2–5 doses of antibodies unlikely to affect brain function) during the first 5 days of onset of neurological manifestations. Patients did not receive specific medication or treatment at time of scan.

In the ZIKV-CNS-GBS, the onset of neurological symptoms occurred within 2 to 30 days (mean = 8.85 days ± 8.03) following a rapid onset after the instauration of febrile symptoms associated with ZIKV infection, in a para-infectious pattern. Upon admission to the neurology service, recent ZIKV infection was confirmed through immunologic testing (IgM/IgG enzyme-linked immunosorbent assay (ELISA) serum levels > 1.1 mg/dL), while Herpes Simplex 1 (HSV-1) was excluded. Other potential febrile syndrome etiologies (Dengue, Chikungunya, Malaria, Leptospirosis, Mononucleosis infecciosa, and HIV primo infection) were ruled out using immunological tests according to the febrile syndromes protocol of the Dominican Republic. Venereal Disease Research Laboratory (VDRL) testing was performed to exclude spirochete-related CNS diseases (e.g., syphilis, Lyme's); all resulting non-reactive. Treating neurologists also excluded other conditions with potential CNS involvement, including viral encephalitis, acute disseminated encephalomyelitis (ADEM), and meningitis, based on clinical presentation, cerebrospinal fluid (CSF) analysis, and electromyography (EMG) findings. The neuroimaging scan was conducted at the chronic stage (12 months ± 10.18 after the initial MRI assessment), during which both CNS and PNS symptoms were evaluated (see Table 1).

In the NZIKV-GBS group, the onset of neurological symptoms occurred without evidence of recent ZIKV infection, as demonstrated by negative immunological testing. Similar to the ZIKV-CNS-GBS group, HSV-1 and other potential causes of febrile illness were ruled out. VDRL testing, to rule out diseases such as syphilis and Lyme disease, was non-reactive for all patients in this group. Additionally, treating neurologists excluded other CNS conditions, including viral encephalitis, ADEM, and meningitis, based on clinical presentation, CSF analysis, and EMG findings. The neuroimaging scan was performed at the chronic stage (10.95 months ± 9.58 after the initial onset of the GBS-associated neurological symptoms), with both CNS and PNS symptoms assessed at the same time (see Table 1).

The healthy control group consisted of individuals with no history of neurological disorders, recent infections, or febrile illnesses.

Table 1. Clinical manifestations of chronic-stage ZIKV-CNS-GBS and NZIKV-GBS patients in the study.

Manifestations	**ZIKV-CNS-GBS (n = 14)**	**NZIKV-GBS (n = 15)**
Central Nervous System (CNS)		
Bitemporal Hemianopsia		
Ophthalmoplegia	1	
Sialorrhea	1	
Hands Dystonia	1 (bilateral)	
Central facial palsy	3	2
Fatigue	1	
Headache	3	4
Loss of visual acuity	1	5
Photophobia	1	1
Peripheral Facial Paresis	1 (right)	
Short-term Memory Disturbances	1	
Peripheral Nervous System (PNS)		
Calf pain	1	
Dysphonia	1	

Upper Limb weakness	2 (1 distal)	
Areflexia	5	14
Dysesthesia	8 (1 all limbs, 1 right limb)	7
Loss of sphincter tone	5	10
Muscular atrophy		2
Paraplegia	2	6
Paresthesia	1	5
Tetraparesis	3	10

Values represent the number of patients exhibiting each manifestation within the specified group. Individual patients may present with more than one manifestation. Symptoms were assessed at the chronic stage, concurrent with the neuroimaging scan.

2.2. MRI data acquisition

All MRI data were acquired on a 3 Tesla Philips Achieva scanner (Philips Healthcare, Best, The Netherlands) at CEDIMAT facilities. We acquired T1-weighted Sagittal MPRAGE sequence (TR/TE = 3000/2.6 ms, flip angle = 90°, voxel size = 1 × 1 × 1 mm^3, 180 slices), T2-weighted axial Fluid Attenuation Inversion Recovery (FLAIR) sequence (TR/TE = 11000/120 ms, inversion time (TI) = 2800 ms, flip angle = 120°, voxel size = 1 × 1 × 1 mm^3, 150 slices), and 6 min eyes-closed resting-state functional MRI (fMRI) using T2-weighted EPI sequence (TR/TE = 2000/30 ms, in-plane matrix size = 80 × 80, flip angle = 80°, voxel size = 2.38 × 2.4 × 3 mm^3 without slice gap, 34 axial slices aligned to AC-PC plane). Diffusion tensor imaging (DTI) was acquired using a single shot, diffusion weighted spin-echo EPI sequence (EPI factor = 67, TR/TE = 5900/60 ms, flip angle = 90°, voxel size = 2 × 2 × 2 mm^3 without slice gap, 33 contiguous slices, in-plane matrix size = 128 × 128, water-fat shift (WFS)/bandwidth (BW) = 20.027 pixels/21.7 Hz, BW in EPI frequency direction = 2502.6 Hz, and total scan time = 4.33 min). Maximum *b*-value was 1000 s/mm^2 in 32 diffusion-weighted directions, and one volume was acquired without diffusion weighting (b_0 = 0 s/mm^2).

2.3. Tract-Based Spatial Statistics

We processed the diffusion imaging data using FSL (FMRIB Software Library) packages and employed the tract-based spatial statistics (TBSS) method (Smith et al., 2006) to derive diffusion tensor parameters: fractional anisotropy (FA) and mean diffusivity (MD). Briefly, eddy-current and motion corrections were applied, followed by fitting the diffusion tensor to the raw diffusion data to calculate FA and MD maps using default parameters (Smith, 2002; Smith et al., 2006; Jenkinson et al., 2012). The FA images were aligned to a 1×1×1 mm^3 FMRIB58_FA standard space, and individual FA images were projected onto the mean fiber tract skeleton. Similarly, all MD images were warped to a common space using the non-linear registration created from the FA analysis. The warped MD images of all subjects were merged into a 4-dimensional file and projected onto the original mean FA skeleton. The resulting FA and MD images were then fed into voxel-wise cross-subject statistics.

2.4. Preprocessing of functional and anatomical MRI data

The preprocessing of functional MRI (fMRI) data was conducted using *fMRIPrep* (version 22.0.2; (Esteban et al., 2019)), an analysis-agnostic pipeline that minimizes manual intervention and optimizes data quality. Briefly, anatomical preprocessing involved skull-stripping of T1-weighted images using Advanced Normalization Tools (ANTs), followed by segmentation into gray matter, white matter, and cerebrospinal fluid with FSL's FAST (Zhang et al., 2001), and cortical surface reconstruction via FreeSurfer (Dale et al., 1999; Fischl, 2012). Spatial normalization was performed to MNI152NLin6Asym and MNI152NLin2009cAsym templates using ANTs. Functional preprocessing included generating a

BOLD reference image, correcting for head motion using FSL's MCFLIRT (Jenkinson et al., 2002), and slice-timing correction with AFNI (Cox and Hyde, 1997). Susceptibility distortion correction was applied using either field maps or a fieldmap-less method based on T1-weighted image registration, followed by alignment of BOLD images to T1-weighted data with boundary-based registration (Greve and Fischl, 2009). The functional data were resampled to both native and standard MNI spaces with minimal smoothing.

2.5. Surface-based morphometry

Surface-based morphometry (SBM) was conducted to derive whole-brain morphometric measures using the default preprocessing steps of the Computational Anatomy Toolbox (CAT12 version 12.8.1) implemented in SPM12 (version 7771). Briefly, the high-resolution MPRAGE T1 data were segmented, and brain surface meshes were registered to the 'FsAverage' template in FreeSurfer. After topology correction, spherical mapping and spherical registration were conducted using the DARTEL algorithm. The Projection-based Thickness (PBT) method was then used to estimate Cortical Thickness by calculating the distance between the gray matter and white matter boundaries (Dahnke et al., 2013). Unlike voxel-based morphometry (VBM), which provides a composite measure of gray matter density and volume, PBT allows for the separation of Cortical Thickness, surface area, and folding. This reduces the partial volume effects inherent to VBM and provides more accurate and sensitive measurements of localized changes in cortical structures (Hutton et al., 2009; Riccelli et al., 2017). The Cortical Thickness maps for the left and right hemispheres were resampled into template space and smoothed using a 15-mm full-width at half-maximum (FWHM) Gaussian kernel.

2.6. Lesion segmentation

Cerebral white matter lesions appear as hyperintensities on FLAIR images. We used a semi-automatic lesion prediction algorithm (LPA) (Schmidt, 2017), implemented in the SPM12-based Lesion Segmentation Toolbox (LST version 3.0.0), that provides automatic lesion filling on the MPRAGE T1-coregistered FLAIR images without needing parameter optimization or binary thresholding of the lesion masks using the logistic regression approach. The resulting lesion probability maps provided two main parameters: Total Lesion Volume (ml) and a Total Number of Lesions.

2.7. Seed-based functional connectivity analysis

Seed-based functional connectivity analysis was conducted with a focus on the hippocampus as a seed due to its known susceptibility to the ZIKV (see introduction). We used the *CONN* toolbox (release 22.v2407) and SPM release 12.7771. The *fMRIPrep*-processed functional data, along with FreeSurfer-segmented anatomical data, were imported into *CONN*. A Gaussian kernel of 6mm with full width at half maximum (FWHM) was used to smooth the functional data for coherence enhancement. Seed-to-voxel correlations were computed by extracting average time series from the region-of-interests (ROIs) and correlating them with all brain voxels, with Fisher z-transformation applied to improve normality. Specifically, the ROIs were defined as bilateral hippocampal areas using the Automated Anatomical Atlas 3 (AAL3; (Rolls et al., 2020)). These ROIs were chosen based on the hypothesis that the progenitor-targeting ZIKV will affect hippocampal area where adult neurogenesis occurs in human brain (Li et al., 2016; Moreno-Jiménez et al., 2021).

2.8. Statistical analysis

For each diffusion parameter (FA and MD), we conducted a non-parametric one-way ANCOVA, adjusting for age and sex, using the threshold-free cluster enhancement (TFCE) approach (Smith and Nichols, 2009). The TFCE method involved 5000 randomized permutations, with a family-wise error (FWE) corrected significance threshold of $p < 0.05$. This produced maps of multiple comparisons-

corrected, cluster-enhanced statistics across space. Cluster coordinates and white matter tract labels were identified using the JHU-ICBM-DTI-81 WM atlas.

We investigated group differences in Cortical Thickness using a one-way ANCOVA with three levels (ZIKV-CNS-GBS, NZIKV-GBS, and healthy controls), adjusting for age and sex. This analysis was implemented using SPM12. Statistical significance was determined with a voxel-level threshold of FWE $p < 0.05$ and a cluster-level threshold of uncorrected $p < 0.05$.

Group differences in white matter lesion parameters (Total Lesion Volume and Total Number of Lesions) were tested using a one-way ANCOVA with three levels, adjusted for age, sex, and TIV, implemented using JASP (version 0.16.2).

For each seed (left and right hippocampus), we conducted a one-way ANCOVA with three levels, adjusting for age, sex, and head motion (mean framewise displacement (FD); Power et al., 2014). Statistical significance was determined with a voxel-level threshold of FWE $p < 0.05$ and a cluster-level threshold of uncorrected $p < 0.05$. Note that the one-way ANCOVA of the factor group, adjusted for age and sex, on the mean FD (Power et al., 2014) revealed no significant difference in head motion among the groups: $F(_{2,\ 31}) = 1.10$, $P = 0.345$.

3. Results

3.1. Adult ZIKV-CNS-associated Changes in White Matter Microstructure

We assessed white matter microstructural properties using two diffusion-tensor scalars, FA and MD. FA measures directional diffusion, reflecting white matter cohesion, while MD provides a directionality-independent measure of diffusivity, sensitive to changes in myelin and intra/extracellular space (Vuoksimaa et al., 2016). Lower FA indicates reduced anisotropic diffusion, while lower MD suggests more restriction to diffusion across all directions. A one-way ANCOVA was conducted for each scalar to examine group differences, corrected for age and sex (TFCE-corrected P (P_{TFCE}) < .05; Figure 2A). Note that with 43 subjects across three groups and two covariates (i.e., age and sex), this ANCOVA has 80% power to detect a large effect size ($f = 0.49$ at an uncorrected error probability of 0.05).

Significant group differences were observed in MD. Subsequently, *post hoc t*-tests were performed to explore ZIKV-CNS-specific white matter microstructural changes (Figure 2B). Specifically, the ZIKV-CNS-GBS showed significantly lower values compared to the healthy controls in the left inferior fronto-occipital fasciculus (26 mm^3; $P_{Peak} = .002$; MNI_{Peak} = -22, 28, -4; Figure 2B, upper right) and the left forceps major (21 mm^3; $P_{TFCE} = .004$; MNI_{Peak} = -12, -42, 19; Figure 2B, upper left). Similarly, the ZIKV-CNS-GBS group had lower MD values than the NZIKV-GBS group in the same areas: the left inferior fronto-occipital fasciculus (26 mm^3; $P_{TFCE} = .002$; MNI_{Peak} = -22, 28, -4; Figure 2B, bottom right) and the left forceps major (26 mm^3; $P_{TFCE} = .002$; MNI_{Peak} = -12, -42, 18; Figure 2B, bottom left).

Furthermore, *post hoc* analyses were conducted to assess GBS-associated changes in white matter microstructural integrity (*Figure S1*). *The post hoc* t-tests revealed that, compared to healthy controls, the NZIKV-GBS group demonstrated higher MD in the left forceps major (25 mm^3; $P_{TFCE} = .008$; MNI_{Peak} = -13, -44, 19).

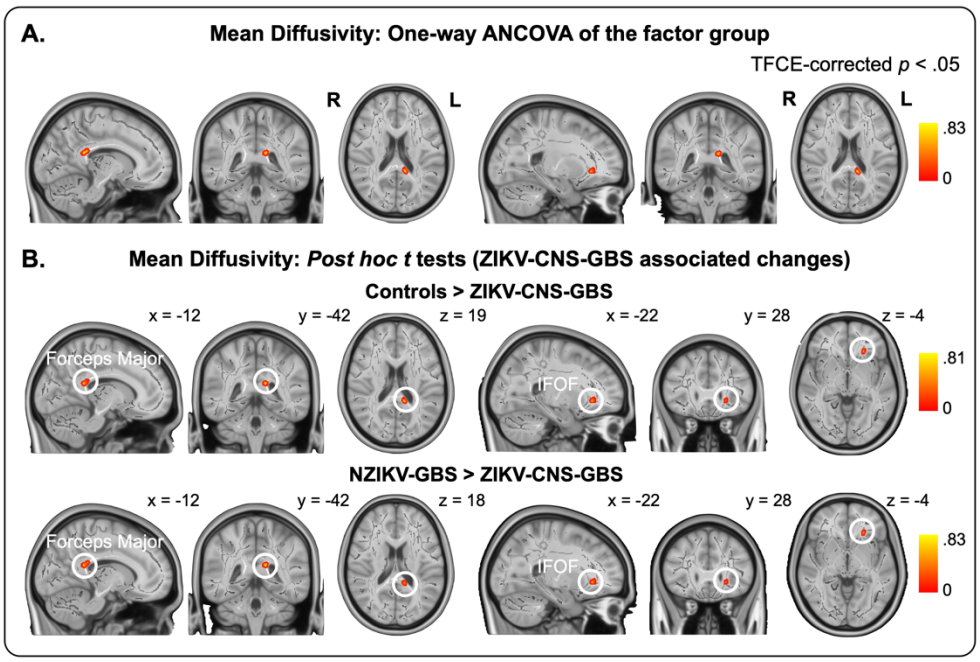

Figure 2. ZIKV-CNS-Associated Changes in White Matter Integrity. [A] A one-way ANCOVA, adjusted for age and sex (A, top panel), identified significant group differences in mean diffusivity (MD) across the groups (ZIKV-CNS-GBS, NZIKV-GBS, and healthy controls) at TFCE-corrected $P < .05$. **[B]** *Post hoc t*-tests showed decreased MD in ZIKV-CNS-GBS group compared to both the healthy controls and NZIKV-GBS groups. Significant clusters are marked with white circles. MNI coordinates (x, y, z) are provided for the peak voxel of each significant cluster. L: left hemisphere, R: right hemisphere, IFOF: inferior fronto-occipital fasciculus.

3.2. Lack of Evidence for Adult ZIKV-CNS-associated Changes in Cortical Thickness

The one-way ANCOVA of the factor group on Cortical Thickness did not reveal significant differences among the groups. With 43 subjects across three groups and two covariates (i.e., age and sex), this ANCOVA had 80% power to detect a large effect size $f = 0.49$ at an uncorrected error probability of 0.05. The null result thus indicates the absence of at least a large effect.

3.3. Lack of Evidence for Adult ZIKV-CNS-associated Changes in White Matter Hyperintensities

White matter regions with hyperintensities were identified using an automated FLAIR-based LPA method. Due to missing FLAIR scans, one ZIKA-CNS-GBS patient and one healthy control subject were excluded, resulting in a total of 41 subjects for statistical analysis. Visual inspection of the white matter lesion maps revealed that most hyperintensities were located in the periventricular regions. However, there was no evidence to support the presence of ZIKV-associated white matter lesions. A one-way ANCOVA for Total Lesion Volume ($F_{(2, 36)} = .457$, $P = 0.637$, $^2_p = 0.025$) and Total Number of Lesions ($F_{(2, 36)} = .128$, $P = 0.880$, $^2_p = 0.007$) showed no significant group differences. With 41 subjects across three groups and three covariates (i.e., age, sex, and TIV), this ANCOVA had 80% power to detect a large effect size $f = 0.51$ at an uncorrected error probability of 0.05. Therefore, the null result suggests that a large effect is unlikely to be present.

To directly assess the likelihood of the null hypothesis, we calculated Bayes Factor (BF) values (H_0: no group effect) versus the alternative hypothesis (H_1). The Bayes Factor for Total Lesion Volume

(BF_{01} = 3.94) and Total Number of Lesions (BF_{01} = 4.57) provided moderate evidence in favor of H_0, suggesting that the data are more likely to occur under the null hypothesis than under the alternative. In contrast and as expected, there was a strong effect of age on white matter lesions: Total Lesion Volume ($F_{(1, 36)}$ = 5.32, P = 0.027, η^2_p = 0.129) and Total Number of Lesions ($F_{(1, 36)}$ = 9.26, P = 0.004, η^2_p = 0.205). Full information on the Total Number of Lesions and Total Lesion Volume of the subjects is reported in *Table S1*.

3.4. Lack of Evidence for Adult ZIKV-CNS-associated Changes in Seed-based FC

Due to missing functional data from five NZIKV-GBS patients and two ZIKV-CNS-GBS patients, 36 subjects were included in the analysis. For both seeds, the one-way ANCOVA of the factor group on seed-based functional connectivity did not reveal significant differences among the groups. With 36 subjects across three groups and three covariates (i.e., age, sex, and mean FD), this ANCOVA has 80% power to detect a large effect size f = 0.54 at an uncorrected error probability of 0.05. The null result therefore shows the absence of large differences across groups.

4. Discussion

The long-term neurological consequences of ZIKV infection have been overlooked in the adult population. While extensive research on ZIKV has focused on fetal and pediatric outcomes, little is known about the sequale in adults. This knowledge gap is pressing, especially with the increasing risk of outbreaks expanding to new regions due to climate change and diverse hosts that can act as viral reservoirs—including mosquitoes, animals, and humans (Vorou, 2016; Munoz et al., 2017; Campos et al., 2020; Baldwin et al., 2021). Our study reveals that adults are also susceptible to significant structural and functional brain changes following infection, underscoring the critical need to broaden the scope of ZIKV research to include adult populations.

Specifically, the urgency to characterize the manifestations in the brain of adults infected with ZIKV arises from the scarcity of systematic research and the absence of vaccines to mitigate its effects on the CNS. Accordingly, our study investigates ZIKV-associated brain manifestations using a comprehensive set of neuroimaging measures, such as cortical thickness, white matter lesions, white matter tractography, and functional connectivity changes. In parallel, we identified brain manifestations associated with general GBS etiology (see *Supplementary Materials*). To our knowledge, our findings provide the first evidence for structural changes associated with the chronic phase of ZIKV-CNS manifestations and GBS etiology.

Diffusion measures, such as FA and MD, are widely interpreted as indicators of cellular microstructure, with reduced FA and increased MD typically interpreted as disrupted fiber tracts and demyelination (Pasi et al., 2016). However, our findings reveal an association between *decreased* MD in the inferior fronto-occipital fasciculus (IFOF) and forceps major and ZIKV-CNS manifestation (Figure 3C). A decrease in MD is often attributed to increased cellularity due to processes like astrogliosis, which involves the proliferation of glial cells, likely as a response to inflammation (Tu et al., 2016), or conditions that restrict extracellular space, such as cytotoxic edema (Noguerol et al., 2020). Notably, reductions in MD have also been observed across a range of pathological states, including multiple sclerosis (Chen et al., 2024), high-grade gliomas, and metastatic brain tumors (Lu et al., 2003). Furthermore, decreased MD has been linked to early inflammatory responses that precede microstructural degradation and macrostructural atrophy, as seen in pre-symptomatic Alzheimer's disease (Weston et al., 2015).

The IFOF is a major white matter tract connecting the frontal, parietal, and occipital lobes, playing a crucial role in integrating visual processing, attention, and executive functions (Sarubbo et al., 2013).

Disruptions in the integrity of the IFOF can impair attentional control and working memory functions by attenuating connections between cortical regions crucial for these cognitive processes (Conner et al., 2018; Gonzalez Alam et al., 2024). Specifically, the IFOF's involvement in the communication between frontal and posterior regions has been implicated in working memory function and Alzheimer's disease (Migliaccio et al., 2012; Overman et al., 2021). Therefore, the CNS symptom observed in our ZIKV-CNS patients—such as short-term memory disturbances (Table 1)— aligns with the functional domains supported by the IFOF. In addition, this finding could suggest a potential etiology or contribution from the CNS to symptoms that were categorized as likely peripheral (i.e., dysesthesia) as it is canonically assumed in the setting of radiculopathies (i.e., GBS), but could be the translation of altered multisensory integration.

Similarly, the forceps major, a component of the corpus callosum, consists of fibers passing through the splenium to connect the occipital lobes bilaterally (Goldstein et al., 2017). This tract is critical for interhemispheric communication, facilitating depth perception, visuospatial coordination, and the integration of visual information across hemispheres. CNS symptoms such as loss of visual acuity and bitemporal hemianopsia (Table 1) are consistent with functional impairments associated with the forceps major, further suggesting the impact of ZIKV infection on key visuospatial pathways. The consistency of the reported symptoms and the functional roles of the IFOF and the forceps major suggests that these regions may serve as a neuroanatomical substrate for the visuo-motor and cognitive impairments observed in ZIKV-CNS patients.

Recent studies have shed light on the mechanisms by which ZIKV infection affects white matter structures. An *in vitro* study using mature murine CNS cultures demonstrated that ZIKV infection causes damage to myelinated fibers and axonal pathology, primarily as a result of oligodendrocyte infection (Schultz et al., 2021b). This highlights the virus's direct impact on myelin-producing cells. Additionally, ZIKV infection in the mature CNS has been shown to induce enhanced microgliosis, a process where activated microglia accumulate in response to injury, and increase production of pro-inflammatory cytokines such as TNF-α (Figueiredo et al., 2019). These inflammatory responses, which activate both microglia and astrocytes, can significantly impact the formation and maintenance of myelin in white matter tracts (Schultz et al., 2021a). Consequently, the observed disruption of white matter microstructures, including the IFOF and the forceps major, in adult ZIKV patients may be attributed to the virus's pro-inflammatory effects on the brain, leading to both direct and indirect damage to myelinated structures. Notably, one of the findings in our prior study was that patients with ZIKV had an atypical GBS presentation (Bido-Medina et al., 2018) and these non-classical forms of GBS are commonly associated with atypical pathophysiological characteristics (Rivera-Correa et al., 2019; Davies et al., 2022), such as the presence of antibodies to myelin glycolipids, pointing towards a parainfectious humoral response that directly impacts myelin.

While our previous work on subacute-phase ZIKV-CNS-GBS patients (Bido-Medina et al., 2018) observed volumetric changes in the gray matter, the current study, which examines chronic-phase patients (i.e., one year after the onset of neurological symptoms; see *Table S1*), did not reveal significant changes in cortical thickness. This contrast raises the possibility that the gray matter changes observed in the subacute phase were part of a transient neuroinflammatory response that resolved over time. Studies on ZIKV have shown that adult patients can experience neurological complications, such as encephalitis and meningitis (da Silva et al., 2017), which can lead to inflammatory processes in the brain. However, in chronic-phase patients, any structural alterations may have stabilized, making it less likely to detect significant differences in cortical thickness at this later stage.

Our findings of prolonged alterations in white matter microstructures, with no significant changes in gray matter, are consistent with evidence that white matter repair is a more complex and resource- and

time-intensive process. White matter recovery depends on the maintenance of long-range axonal integrity and remyelination by oligodendrocytes, which are particularly susceptible to inflammation and oxidative stress, potentially induced by neurotropic ZIKV, due to their intense metabolic demands for lipid synthesis and ATP-dependent myelin maintenance (Shahsavani et al., 2021; Spaas et al., 2021). This process requires two to three times more neuronal energy expenditure than that of gray matter (Connor and Menzies, 1996; Bartzokis, 2004). However, our null findings in grey matter should be interpreted cautiously, as the sample size in this study was sufficiently powered to detect only large effect sizes.

The primary limitation of this study arises from the rarity of ZIKV-infected adult patients who present with CNS manifestations beyond GBS, which leads to a small sample size. Additionally, the goal of controlling for GBS to enhance the specificity of our findings led to challenges in obtaining age- and sex-matched control groups with NZIKV-GBS etiology. This challenge stems from the fact that GBS from non-ZIKV etiology is likewise a rare disorder. As a result of the limited sample size, the study was only powered to detect large effect sizes. Therefore, any potential small or medium effects will have been missed. These limitations notwithstanding, our rigorously controlled analyses revealed abnormalities in the white matter of ZIKV patients with CNS sympotoms.

In conclusion, our study reveals long-term effects of ZIKV infection on the brain's white matter integrity. Together with our previous findings on subacute-phase ZIKV adult patients (Bido-Medina et al., 2018), our findings suggest that ZIKV can induce both acute and long-lasting alterations in brain structure, with a particular impact on white matter microstructure during the chronic phase of infection. Importantly, this study underscores that adults are also vulnerable to the neurological effects of ZIKV infection, a domain that has been predominantly explored in the context of congenital ZIKV infections. These broader neurological consequences of ZIKV have implications for preventative health policy, calling for to incorporation of long-term risks across the full lifespan.

References

Aliota MT, Caine EA, Walker EC, Larkin KE, Camacho E, Osorio JE (2016) Characterization of Lethal Zika Virus Infection in AG129 Mice. PLOS Neglected Tropical Diseases 10:e0004682.

Baldwin WR, Giebler HA, Stovall JL, Young G, Bohning KJ, Dean HJ, Livengood JA, Huang CY-H (2021) Single dose of chimeric dengue-2/Zika vaccine candidate protects mice and non-human primates against Zika virus. Nat Commun 12:7320.

Bartzokis G (2004) Age-related myelin breakdown: a developmental model of cognitive decline and Alzheimer's disease. Neurobiology of Aging 25:5–18.

Bido-Medina R, Wirsich J, Rodriguez M, Oviedo J, Miches I, Bido P, Tusen L, Stoeter P, Sadaghiani S (2018) Impact of Zika Virus on adult human brain structure and functional organization. Ann Clin Transl Neurol 5:752–762.

Bobermin LD, Quincozes-Santos A, Santos CL, Varela APM, Teixeira TF, Wartchow KM, Lissner LJ, da Silva A, Thomaz NK, Santi L, Beys-da-Silva WO, Roehe PM, Sesterheim P, Guimarães JA, Gonçalves C-A, Souza DO (2020) Zika virus exposure affects neuron-glia communication in the hippocampal slices of adult rats. Sci Rep 10:21604.

Büttner C, Heer M, Traichel J, Schwemmle M, Heimrich B (2019) Zika Virus-Mediated Death of Hippocampal Neurons Is Independent From Maturation State. Front Cell Neurosci 0 Available at: https://www.frontiersin.org/articles/10.3389/fncel.2019.00389/full [Accessed July 20, 2021].

Campos GS, Hughes Carvalho R, Bandeira AC, Reboredo-Oliveira L, Dos Santos Costa R, Figueiredo CA, Sardi SI (2020) New Challenge for Zika Virus Infection: Human Reservoirs? Viral Immunol 33:489–492.

Cao-Lormeau VM et al. (2016) Guillain-Barre Syndrome outbreak associated with Zika virus infection in French Polynesia: a case-control study. Lancet 387:1531–1539.

Carteaux G, Maquart M, Bedet A, Contou D, Brugieres P, Fourati S, Cleret de Langavant L, de Broucker T, Brun-Buisson C, Leparc-Goffart I, Mekontso Dessap A (2016) Zika Virus Associated with Meningoencephalitis. N Engl J Med 374:1595–1596.

Chen X, Roberts N, Zheng Q, Peng Y, Han Y, Luo Q, Feng J, Luo T, Li Y (2024) Comparison of diffusion tensor imaging (DTI) tissue characterization parameters in white matter tracts of patients with multiple sclerosis (MS) and neuromyelitis optica spectrum disorder (NMOSD). Eur Radiol 34:5263–5275.

Conner AK, Briggs RG, Sali G, Rahimi M, Baker CM, Burks JD, Glenn CA, Battiste JD, Sughrue ME (2018) A Connectomic Atlas of the Human Cerebrum—Chapter 13: Tractographic Description of the Inferior Fronto-Occipital Fasciculus. Operative Neurosurgery 15:S436–S443.

Connor JR, Menzies SL (1996) Relationship of iron to oligondendrocytes and myelination. Glia 17:83–93.

Cox RW, Hyde JS (1997) Software tools for analysis and visualization of fMRI data. NMR in Biomedicine 10:171–178.

da Silva IRF, Frontera JA, Bispo de Filippis AM, Nascimento O, Group R-G-ZR (2017) Neurologic Complications Associated With the Zika Virus in Brazilian Adults. JAMA Neurol 74:1190–1198.

Dahnke R, Yotter RA, Gaser C (2013) Cortical thickness and central surface estimation. NeuroImage 65:336–348.

Dale AM, Fischl B, Sereno MI (1999) Cortical Surface-Based Analysis: I. Segmentation and Surface Reconstruction. NeuroImage 9:179–194.

Davies AJ et al. (2022) Guillain-Barré Syndrome Following Zika Virus Infection Is Associated With a Diverse Spectrum of Peripheral Nerve Reactive Antibodies. Neurol Neuroimmunol Neuroinflamm 10:e200047.

Devhare P, Meyer K, Steele R, Ray RB, Ray R (2017) Zika virus infection dysregulates human neural stem cell growth and inhibits differentiation into neuroprogenitor cells. Cell Death Dis 8:e3106–e3106.

Dos Santos T et al. (2016) Zika Virus and the Guillain-Barre Syndrome - Case Series from Seven Countries. N Engl J Med 375:1598–1601.

Dowall SD, Graham VA, Rayner E, Atkinson B, Hall G, Watson RJ, Bosworth A, Bonney LC, Kitchen S, Hewson R (2016) A Susceptible Mouse Model for Zika Virus Infection. PLOS Neglected Tropical Diseases 10:e0004658.

Esteban O, Markiewicz CJ, Blair RW, Moodie CA, Isik AI, Erramuzpe A, Kent JD, Goncalves M, DuPre E, Snyder M, Oya H, Ghosh SS, Wright J, Durnez J, Poldrack RA, Gorgolewski KJ (2019) fMRIPrep: a robust preprocessing pipeline for functional MRI. Nat Methods 16:111–116.

Figueiredo CP et al. (2019) Zika virus replicates in adult human brain tissue and impairs synapses and memory in mice. Nat Commun 10:3890.

Fischl B (2012) FreeSurfer. Neuroimage 62:774–781.

Galliez RM, Spitz M, Rafful PP, Cagy M, Escosteguy C, Germano CS, Sasse E, Goncalves AL, Silveira PP, Pezzuto P, Ornelas AM, Tanuri A, Aguiar RS, Moll FT (2016) Zika Virus Causing Encephalomyelitis Associated With Immunoactivation. Open Forum Infect Dis 3:ofw203.

Garber C, Soung A, Vollmer LL, Kanmogne M, Last A, Brown J, Klein RS (2019) T cells promote microglia-mediated synaptic elimination and cognitive dysfunction during recovery from neuropathogenic flaviviruses. Nat Neurosci 22:1276–1288.

Goldstein A, Covington BP, Mahabadi N, Mesfin FB (2017) Neuroanatomy, Corpus Callosum. StatPearls Publishing, Treasure Island (FL). Available at: http://europepmc.org/books/NBK448209.

Gonzalez Alam TRJ, Cruz Arias J, Jefferies E, Smallwood J, Leemans A, Marino Davolos J (2024) Ventral and dorsal aspects of the inferior frontal-occipital fasciculus support verbal semantic access and visually-guided behavioural control. Brain Struct Funct 229:207–221.

Greve DN, Fischl B (2009) Accurate and robust brain image alignment using boundary-based registration. NeuroImage 48:63–72.

Hutton C, Draganski B, Ashburner J, Weiskopf N (2009) A comparison between voxel-based cortical thickness and voxel-based morphometry in normal aging. Neuroimage 48:371–380.

Jenkinson M, Bannister P, Brady M, Smith S (2002) Improved Optimization for the Robust and Accurate Linear Registration and Motion Correction of Brain Images. NeuroImage 17:825–841.

Jenkinson M, Beckmann CF, Behrens TEJ, Woolrich MW, Smith SM (2012) FSL. NeuroImage 62:782–790.

Jeong GU, Lee S, Kim DY, Lyu J, Yoon GY, Kim K-D, Ku KB, Ko J, Kwon Y-C (2023) Zika Virus Infection Induces Interleukin-1β-Mediated Inflammatory Responses by Macrophages in the Brain of an Adult Mouse Model. J Virol 97:e00556-23.

Kim J, Alejandro B, Hetman M, Hattab EM, Joiner J, Schroten H, Ishikawa H, Chung D-H (2020) Zika virus infects pericytes in the choroid plexus and enters the central nervous system through the blood-cerebrospinal fluid barrier. PLOS Pathogens 16:e1008204.

Koma T, Veljkovic V, Anderson DE, Wang L-F, Rossi SL, Shan C, Shi P-Y, Beasley DW, Bukreyeva N, Smith JN, Hallam S, Huang C, von Messling V, Paessler S (2018) Zika virus infection elicits auto-antibodies to C1q. Sci Rep 8:1882.

Kumar A, Singh HN, Pareek V, Raza K, Dantham S, Kumar P, Mochan S, Faiq MA (2016) A Possible Mechanism of Zika Virus Associated Microcephaly: Imperative Role of Retinoic Acid Response Element (RARE) Consensus Sequence Repeats in the Viral Genome. Front Hum Neurosci 10:403.

Leda AR, Bertrand L, Andras IE, El-Hage N, Nair M, Toborek M (2019) Selective Disruption of the Blood–Brain Barrier by Zika Virus. Front Microbiol 10:2158.

Li H, Saucedo-Cuevas L, Regla-Nava JA, Chai G, Sheets N, Tang W, Terskikh AV, Shresta S, Gleeson JG (2016) Zika Virus Infects Neural Progenitors in the Adult Mouse Brain and Alters Proliferation. Cell Stem Cell 19:593–598.

Lu S, Ahn D, Johnson G, Cha S (2003) Peritumoral Diffusion Tensor Imaging of High-Grade Gliomas and Metastatic Brain Tumors. American Journal of Neuroradiology 24:937–941.

Migliaccio R, Agosta F, Toba MN, Samri D, Corlier F, de Souza LC, Chupin M, Sharman M, Gorno-Tempini ML, Dubois B, Filippi M, Bartolomeo P (2012) Brain networks in posterior cortical atrophy: A single case tractography study and literature review. Cortex 48:1298–1309.

Moreno-Jiménez EP, Terreros-Roncal J, Flor-García M, Rábano A, Llorens-Martín M (2021) Evidences for Adult Hippocampal Neurogenesis in Humans. J Neurosci 41:2541–2553.

Munoz LS, Barreras P, Pardo CA (2016) Zika Virus-Associated Neurological Disease in the Adult: Guillain-Barre Syndrome, Encephalitis, and Myelitis. Semin Reprod Med 34:273–279.

Munoz LS, Parra B, Pardo CA, Neuroviruses Emerging in the Americas S (2017) Neurological Implications of Zika Virus Infection in Adults. J Infect Dis 216:S897–S905.

Noguerol TM, Barousse R, Amrhein TJ, Royuela-del-Val J, Montesinos P, Luna A (2020) Optimizing Diffusion-Tensor Imaging Acquisition for Spinal Cord Assessment: Physical Basis and Technical Adjustments. RadioGraphics 40:403–427.

Overman MJ, Zamboni G, Butler C, Ahmed S (2021) Splenial white matter integrity is associated with memory impairments in posterior cortical atrophy. Brain Communications 3:fcab060.

Papa MP, Meuren LM, Coelho SVA, Lucas CG de O, Mustafá YM, Lemos Matassoli F, Silveira PP, Frost PS, Pezzuto P, Ribeiro MR, Tanuri A, Nogueira ML, Campanati L, Bozza MT, Paula Neto HA, Pimentel-Coelho PM, Figueiredo CP, Aguiar RS de, Arruda LB de (2017) Zika Virus Infects, Activates, and Crosses Brain Microvascular Endothelial Cells, without Barrier Disruption. Front Microbiol 8 Available at: https://www.frontiersin.org/journals/microbiology/articles/10.3389/fmicb.2017.02557/full [Accessed January 9, 2025].

Parra B et al. (2016) Guillain-Barre Syndrome Associated with Zika Virus Infection in Colombia. N Engl J Med 375:1513–1523.

Pasi M, van Uden IWM, Tuladhar AM, de Leeuw F-E, Pantoni L (2016) White Matter Microstructural Damage on Diffusion Tensor Imaging in Cerebral Small Vessel Disease. Stroke 47:1679–1684.

Power JD, Mitra A, Laumann TO, Snyder AZ, Schlaggar BL, Petersen SE (2014) Methods to detect, characterize, and remove motion artifact in resting state fMRI. NeuroImage 84:320–341.

Pradhan F, Burns JD, Agameya A, Patel A, Alfaqih M, Small JE, Ooi W (2017) Case Report: Zika Virus Meningoencephalitis and Myelitis and Associated Magnetic Resonance Imaging Findings. Am J Trop Med Hyg 97:340–343.

Rasmussen SA, Jamieson DJ, Honein MA, Petersen LR (2016) Zika Virus and Birth Defects--Reviewing the Evidence for Causality. N Engl J Med 374:1981–1987.

Riccelli R, Toschi N, Nigro S, Terracciano A, Passamonti L (2017) Surface-based morphometry reveals the neuroanatomical basis of the five-factor model of personality. Social Cognitive and Affective Neuroscience 12:671–684.

Rivera-Correa J, Siqueira IC de, Mota S, Rosário MS do, Jesus PAP de, Alcantara LCJ, Ernst JD, Rodriguez A (2019) Anti-ganglioside antibodies in patients with Zika virus infection-associated Guillain-Barré Syndrome in Brazil. PLOS Neglected Tropical Diseases 13:e0007695.

Rolls ET, Huang C-C, Lin C-P, Feng J, Joliot M (2020) Automated anatomical labelling atlas 3. NeuroImage 206:116189.

Sarubbo S, De Benedictis A, Maldonado IL, Basso G, Duffau H (2013) Frontal terminations for the inferior fronto-occipital fascicle: anatomical dissection, DTI study and functional considerations on a multi-component bundle. Brain Struct Funct 218:21–37.

Schmidt P (2017) Bayesian inference for structured additive regression models for large-scale problems with applications to medical imaging. Available at: https://edoc.ub.uni-muenchen.de/20373/ [Accessed May 16, 2022].

Schultz V, Barrie JA, Donald CL, Crawford CL, Mullin M, Anderson TJ, Solomon T, Barnett SC, Linington C, Kohl A, Willison HJ, Edgar JM (2021a) Oligodendrocytes are susceptible to Zika virus infection in a mouse model of perinatal exposure: Implications for CNS complications. Glia 69:2023–2036.

Schultz V, Cumberworth SL, Gu Q, Johnson N, Donald CL, McCanney GA, Barrie JA, Da Silva Filipe A, Linington C, Willison HJ, Edgar JM, Barnett SC, Kohl A (2021b) Zika Virus Infection Leads to Demyelination and Axonal Injury in Mature CNS Cultures. Viruses 13:91.

Sebastian UU et al. (2017) Zika virus-induced neurological critical illness in Latin America: Severe Guillain-Barre Syndrome and encephalitis. J Crit Care 42:275–281.

Shahsavani N, Kataria H, Karimi-Abdolrezaee S (2021) Mechanisms and repair strategies for white matter degeneration in CNS injury and diseases. Biochimica et Biophysica Acta (BBA) - Molecular Basis of Disease 1867:166117.

Smith SM (2002) Fast robust automated brain extraction. Hum Brain Mapp 17:143–155.

Smith SM, Jenkinson M, Johansen-Berg H, Rueckert D, Nichols TE, Mackay CE, Watkins KE, Ciccarelli O, Cader MZ, Matthews PM, Behrens TE (2006) Tract-based spatial statistics: voxelwise analysis of multi-subject diffusion data. Neuroimage 31:1487–1505.

Smith SM, Nichols TE (2009) Threshold-free cluster enhancement: addressing problems of smoothing, threshold dependence and localisation in cluster inference. Neuroimage 44:83–98.

Souza BSF, Sampaio GLA, Pereira CS, Campos GS, Sardi SI, Freitas LAR, Figueira CP, Paredes BD, Nonaka CKV, Azevedo CM, Rocha VPC, Bandeira AC, Mendez-Otero R, dos Santos RR, Soares MBP (2016) Zika virus infection induces mitosis abnormalities and apoptotic cell death of human neural progenitor cells. Sci Rep 6:39775.

Spaas J, van Veggel L, Schepers M, Tiane A, van Horssen J, Wilson DM, Moya PR, Piccart E, Hellings N, Eijnde BO, Derave W, Schreiber R, Vanmierlo T (2021) Oxidative stress and impaired oligodendrocyte precursor cell differentiation in neurological disorders. Cell Mol Life Sci 78:4615–4637.

Sutarjono B (2019) Can We Better Understand How Zika Leads to Microcephaly? A Systematic Review of the Effects of the Zika Virus on Human Brain Organoids. The Journal of Infectious Diseases 219:734–745.

Tu T-W, Williams RA, Lescher JD, Jikaria N, Turtzo LC, Frank JA (2016) Radiological–pathological correlation of diffusion tensor and magnetization transfer imaging in a closed head traumatic brain injury model. Annals of Neurology 79:907–920.

Vorou R (2016) Zika virus, vectors, reservoirs, amplifying hosts, and their potential to spread worldwide: what we know and what we should investigate urgently. Int J Infect Dis 48:85–90.

Vuoksimaa E, Panizzon MS, Hagler Jr DJ, Hatton SN, Fennema-Notestine C, Rinker D, Eyler LT, Franz CE, Lyons MJ, Neale MC, Tsuang MT, Dale AM, Kremen WS (2016) Heritability of white matter microstructure in late middle age: A twin study of tract-based fractional anisotropy and absolute diffusivity indices. Hum Brain Mapp 38:2026–2036.

Weston PSJ, Simpson IJA, Ryan NS, Ourselin S, Fox NC (2015) Diffusion imaging changes in grey matter in Alzheimer's disease: a potential marker of early neurodegeneration. Alzheimer's Research & Therapy 7:47.

World Health Organization (WHO) (2022) Zika Epidemiology Update.

Zhang Y, Brady M, Smith S (2001) Segmentation of brain MR images through a hidden Markov random field model and the expectation-maximization algorithm. IEEE Transactions on Medical Imaging 20:45–57.

Zhou T, Tan L, Cederquist GY, Fan Y, Hartley BJ, Mukherjee S, Tomishima M, Brennand KJ, Zhang Q, Schwartz RE, Evans T, Studer L, Chen S (2017) High-Content Screening in hPSC-Neural Progenitors Identifies Drug Candidates that Inhibit Zika Virus Infection in Fetal-like Organoids and Adult Brain. Cell Stem Cell 21:274-283.e5.